ADVANCED FUNCTIONAL MATERIALS

Supporting Information

for *Adv. Funct. Mater.*, DOI: 10.1002/adfm.201801617

High Thermoelectric Performance in Supersaturated Solid Solutions and Nanostructured n-Type PbTe–GeTe

Zhong-Zhen Luo, Xiaomi Zhang, Xia Hua, Gangjian Tan, Trevor P. Bailey, Jianwei Xu, Ctirad Uher, Chris Wolverton, Vinayak P. Dravid, Qingyu Yan, and Mercouri G. Kanatzidis**

Supporting Information

High Thermoelectric Performance in Supersaturated Solid Solutions and Nanostructured n-type PbTe-GeTe

Zhong-Zhen Luo, Xiaomi Zhang, Xia Hua, Gangjian Tan, Trevor P. Bailey, Jianwei Xu, Ctirad Uher, Chris Wolverton, Vinayak P. Dravid, Qingyu Yan, Mercouri G. Kanatzidis**

Table S1. Hall carrier concentration (n, 10^{19} cm^{-3}) and mobility (μ_H, $cm^2V^{-1}s^{-1}$) of the $Pb_{0.988}Sb_{0.012}Te$-x%GeTe-SS (x = 0, 2, 5, 8, 10, 12, 13 and 14) samples at 300 K

x	0	2	5	8	10	12	13	14
n	4.93	4.56	3.71	2.50	2.77	1.85	1.44	1.36
μ_H	365.47	332.94	297.08	272.79	221.20	294.80	281.76	274.22

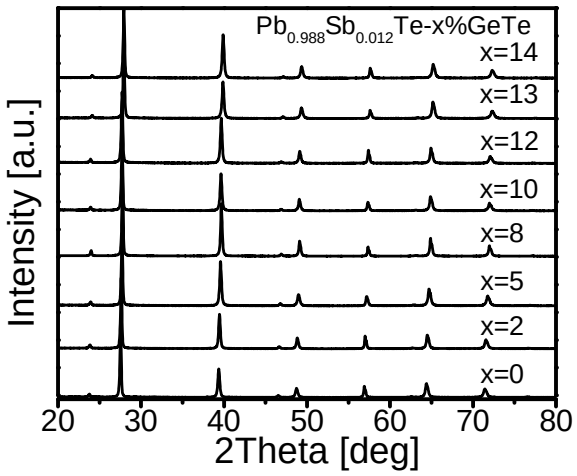

Figure. S1. PXRD patterns of $Pb_{0.988}Sb_{0.012}Te$-x%GeTe-SS (x = 0, 2, 5, 8, 10, 12, 13 and 14) samples with varied doping levels.

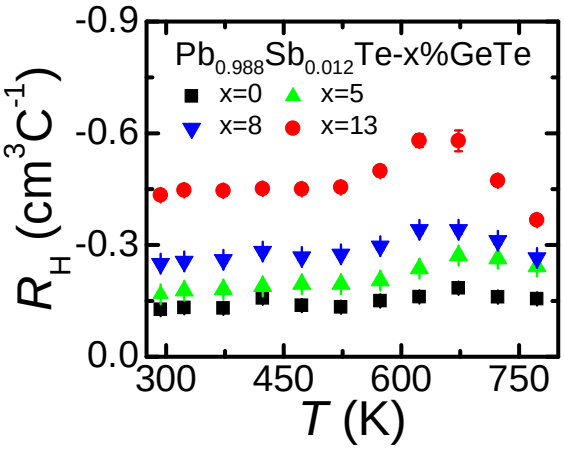

Figure. S2. The temperature-dependence Hall coefficient of n-type $Pb_{0.988}Sb_{0.012}Te$-x%GeTe-SS (x = 0, 5, 8, 13) for $Pb_{0.988}Sb_{0.012}Te$-x%GeTe-SS SPSed pellets.

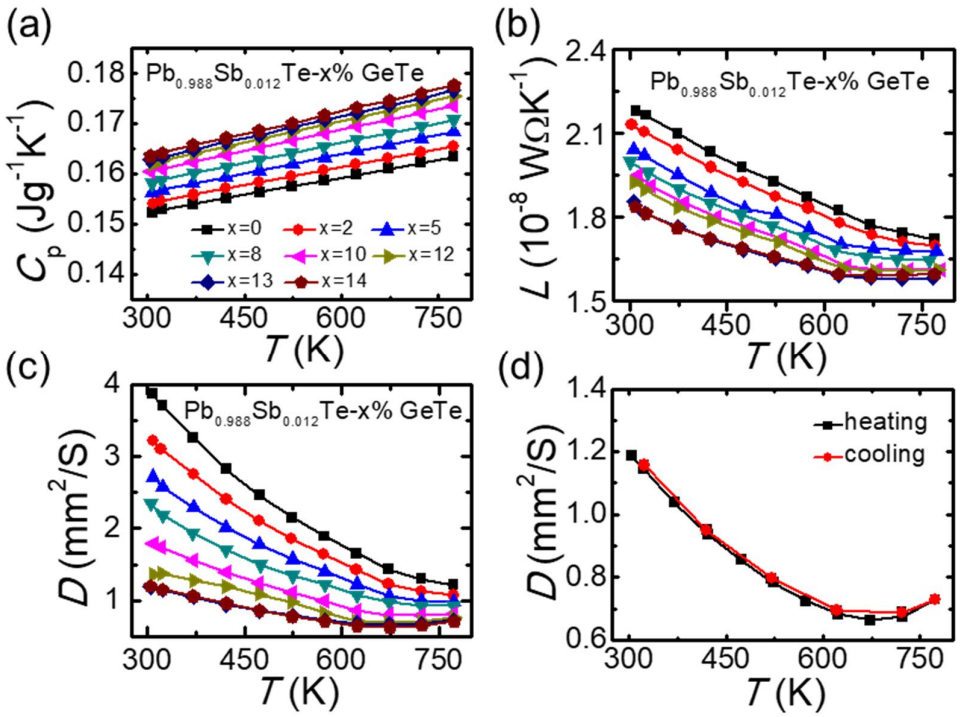

Figure. S3. Temperature-dependent (a) heat capacities, C_p; (b) electronic thermal conductivity, κ_{ele}; (c) Lorenz numbers, L; and (d) thermal diffusivity, D for $Pb_{0.988}Sb_{0.012}Te$-13%GeTe-SS.

Electronic thermal conductivity. To investigate the thermal conductivity further, the electronic and lattice components are evaluated. The electronic thermal conductivity (κ_{ele}) is calculated using the Wiedemann-Franz law,[1] $\kappa_{ele} = L\sigma T$, where L is the Lorenz number and estimated using the equation:

$$L = 1.5 + \exp[-|S|/116] \times 10^{-8}\ V^2/K^2 \quad (1)$$

As shown in Figure 5b, with increasing GeTe content, κ_{ele} decreases due to the reduction of electrical conductivities.

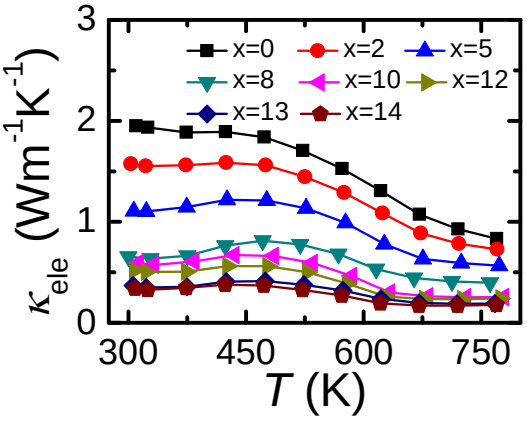

Figure. S4. Electronic thermal conductivity, κ_{ele} for $Pb_{0.988}Sb_{0.012}Te$-x%GeTe-SS.

Table S2. Room temperature densities of $Pb_{0.988}Sb_{0.012}Te$-x%GeTe (x = 0, 2, 5, 8, 10, 12, 13 and 14)

Composition	Measured Density, g/cm^3	Theoretical Density,* %
$Pb_{0.988}Sb_{0.012}Te$	8.002	98.0
$Pb_{0.988}Sb_{0.012}Te$-2%GeTe	8.059	99.2
$Pb_{0.988}Sb_{0.012}Te$-5%GeTe	7.874	97.6
$Pb_{0.988}Sb_{0.012}Te$-8%GeTe	7.930	99.1
$Pb_{0.988}Sb_{0.012}Te$-10%GeTe	7.727	97.0
$Pb_{0.988}Sb_{0.012}Te$-12%GeTe	7.700	97.2
$Pb_{0.988}Sb_{0.012}Te$-13%GeTe-SS	7.659	96.9
$Pb_{0.988}Sb_{0.012}Te$-13%GeTe-Nano	7.605	96.2
$Pb_{0.988}Sb_{0.012}Te$-14%GeTe	7.499	95.1

*The theoretical densities of the $Pb_{0.988}Sb_{0.012}Te$-x%GeTe samples were calculated using the law of mixtures in light of the volume fraction of each component.

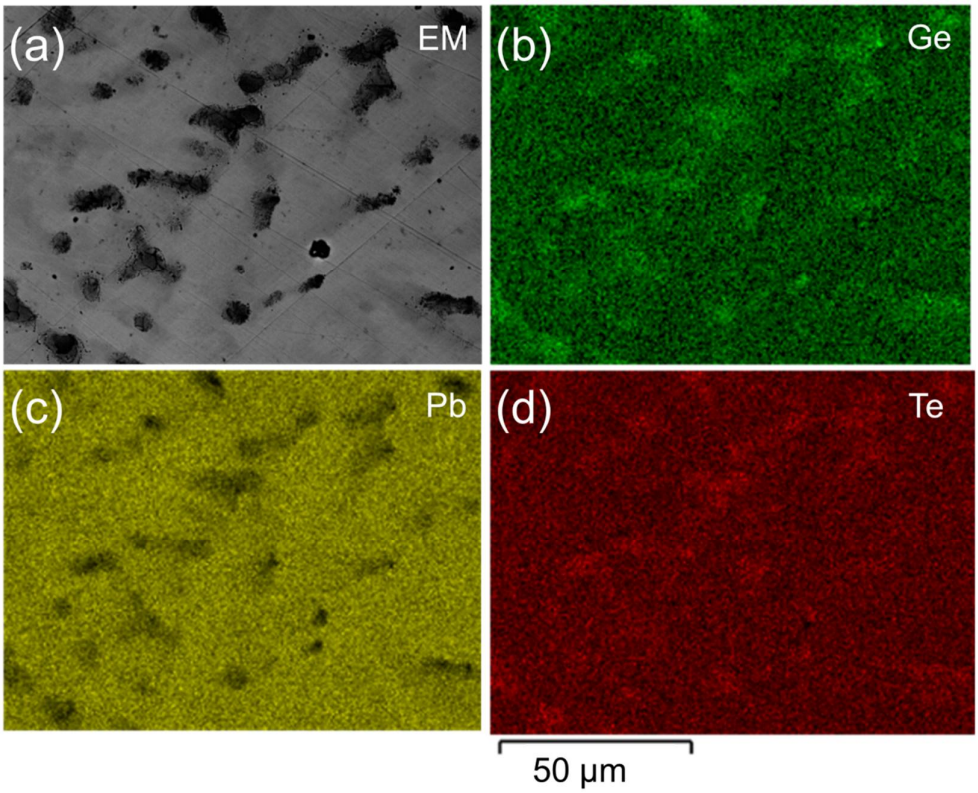

Figure. S5. Backscattered electron (BSE) image and EDS analysis of 573K annealed $Pb_{0.988}Sb_{0.012}Te$-13%GeTe before SPS. (a) BSE image, (b) Ge, (c) Pb and (d) Te elemental maps for the area in (a). The dark phase in (a) are rich in Ge and Te and deficient in Pb. We note that spark plasma sintering can significantly change the microstructure of the 573K annealed $Pb_{0.988}Sb_{0.012}Te$-13%GeTe. Figure S5 depicts that large, microscale second phase which is rich in Ge and Te and deficient in Pb can be observed in the sample before SPS, in contrast to the nanoscale second phase after SPS.